

# Effect of Mn Concentration on Structural, Optical Properties and Humidity Sensing Activity of Tin oxide Nanoparticles

M. Sabarilakshmi<sup>1</sup>, K. Janaki<sup>2</sup>

<sup>1</sup>Department of Physics, Vivekanandha Arts and Science College for Women, Salem -637303 Tamilnadu, India

<sup>2</sup>Department of Physics, Government Arts College for Women, Salem - 636 008, Tamilnadu, India

**Abstract:** The nano structured pure and Mn doped SnO<sub>2</sub> particles were synthesized and their structural, optical and humidity sensing properties were examined. The investigated samples were effectively prepared by hydrothermal method. The X-ray diffraction confirms the tetragonal rutile phase of the nano particles. The structural property of nano particles were analyzed by Transmission electron microscope (TEM) and the result shows the size of the nano particle around 50 nm in both pure and Mn-doped samples. The change in energy gap confirms the substitution of Mn into SnO<sub>2</sub> sites by doping small amount of metal ion. Fourier transform infrared (FTIR) was used to determine functional group. The efficiency and the relationship between the resistance and relative humidity were verified by the humidity sensor analysis.

**Keywords:** Nanoparticles, SnO<sub>2</sub>, hydrothermal, Electrical Properties, Optical Properties

## 1. Introduction

Tin oxide based nano particles playing a vital role in the sensor applications rather than metal oxides. Tin oxide has a rutile type crystal structure with lattice parameters  $a=b=4.75\text{\AA}$  and  $c=3.19\text{\AA}$ . Tin oxide has an energy band gap of  $\sim 3.6\text{ eV}$  [1-3]. SnO<sub>2</sub> has been explored widely due to their potential applications in pH and biosensors [6-11], transparent conducting electrodes [4, 5], lithium ion batteries [6, 7], field effect transistors [8], sensitized solar cells [9, 10], varistors [11], catalysts agent [12], hazardous gas sensors [13], heat reflecting mirrors [14, 15], and optoelectronic devices [16]. Sensors containing metal oxide nano particles typically display high sensitivity compared to their counterparts made of macro sized particles. Crystallite size is one of the prominent factors affecting the sensitivity of humidity sensors. Tin oxide humidity sensors are widely used in daily life and industry due to high stability, low cost and especially high sensitivity. The humidity sensing mechanism is related with change in resistance caused by surface reaction of water vapour with SnO<sub>2</sub> Nano particles [16-17]. Hence, in order to achieve high sensitivity, metal oxides with fine crystallite size are mandatory.

So far, several techniques have been developed to synthesize nanoparticles, by sol-gel method, hydrothermal technique, chemical co-precipitation, microwave irradiation method, and polyol method [18-22]. Among these techniques, hydrothermal method is mostly attractive due to its short preparation time, low temperature synthesis, low cost, high purity and potential advantage for large scale production. Recently, this method is being effectively used for direct synthesis of nano crystalline metal oxide and materials.

Efficiency of tin oxide could be improved by dopant ions. For instance, innovative applications are well documented by doping metal ions such as Cu, Sb, Zn, Mn, F, and Mg. It narrows down the energy gap and increases the conductivity of tin oxide. However, Mn-doped SnO<sub>2</sub> has gained the

attractive feature. It was important to note that energy band gap can be adjusted due to the existence of Mn ions in SnO<sub>2</sub> lattice parameters [22]. Therefore, in this article, it is aimed to synthesis Mn-doped SnO<sub>2</sub> particle by hydrothermal method and investigated for the pure and Mn-doped SnO<sub>2</sub> particles synthesized by hydrothermal method.

## 2. Experimental Procedure

All reagents (analytical grade) were used without any further purification. Tin chloride dihydrate (SnCl<sub>2</sub>·2H<sub>2</sub>O) and Magnesium chloride dihydrate (MnCl<sub>2</sub>·2H<sub>2</sub>O) were used starting materials. Sodium hydroxide (NaOH) solution was used as precipitate agent. The solution of the 0.1 M solution of tin hydroxyl group [Sn(OH)<sup>6-</sup>] of SnO<sub>2</sub> and Mn-doped SnO<sub>2</sub> samples were prepared by dissolving of 2.25 g of SnCl<sub>2</sub>·2H<sub>2</sub>O dissolved in 100 ml of distilled water. The suitable amount of MnCl<sub>2</sub>·2H<sub>2</sub>O (0, 5 and 10 wt %) dissolved in the prepared solution and stirred for 40 min. Consequently, an aqueous NaOH was gradually added drop wise with strong stirring so as to attain the pH of the solution should reach 8. In order to confirm the homogeneity, the dropping rate was systematically controlled. The Cl<sup>-</sup> ions were removed by washing with deionized water and confirmed by silver nitrate test. Then precipitate gel was transferred into a Teflon-lined autoclave for hydrothermal reaction at 100 °C for 15 h and dried at 80 °C for 24 h. Finally, the white and light grey colored pure and Mn doped SnO<sub>2</sub> nanopowders were successively prepared.

### 2.1 Characterization techniques

Crystallite phases present in the samples were identified by X-ray diffraction (XRD) on a Bruker diffractometer using CuK $\alpha$  ( $\lambda = 1.5406$ ) radiation operating at 40 kV and 30 mA at a rate of 2°/min. The diffraction data were recorded for 2 $\theta$  values between 20° and 80°. Transmission electron microscopy (TEM) was performed with a (Technai G20-stwin) high resolution electron microscope (HRTEM) with

Volume 7 Issue 7, July 2018

[www.ijsr.net](http://www.ijsr.net)

Licensed Under Creative Commons Attribution CC BY

an accelerating voltage of 300Kv. The UV-Vis absorption spectrum was measured by a UV-VIS-NIR scanning spectrophotometer (Perkin Elmer UV/VIS/NIR Lambda 19 spectrophotometer) in the range of 200-800nm. The photoluminescence (PL) spectra of SnO<sub>2</sub> were recorded using JASCO FP-6300 spectrofluorometer in the wavelength range of 400-800 nm and excitation wavelength of 350nm. The Fourier transformed infrared spectra (FT-IR) of the samples were collected using a 5DX FTIR Spectrometer.

## 2.2 Humidity sensor set up

The humidity sensor system consists of quartz glass plates with size 300 mm x 300 mm in dimension and 10 mm thickness provided with top and bottom of the glass plates. The two holes were provided in bottom and top of the glass plates in order to insert and remove the water vapour. In the right upper side of the glass reactor, the vacuum pump is attached to humidify the chamber for the next cycle/sample. The electrical resistance of the sensor material has been measured using LCR Bridge under different humidity conditions. The humidity levels are varied from 10-90% RH. The percentage of humidity was measured by using standard hygrometer. Thin films for humidity sensitivity sensors were prepared by using Mn-SnO<sub>2</sub> nano powders. The prepared nano powder was first dispersed in ethanol and the solution is then coated on silicon with a pair of electrode using spin coating method. The electrode contacts were made by silver paste. where  
 The percentage of sensitivity for detection of humidity is defined as [13]

$$S = \frac{RH_2 - RH_1}{RH_1} \times 100$$

Where RH<sub>2</sub> is the resistivity of the sample for humidity at level 2 (highest RH level) and RH<sub>1</sub> is the resistivity of the sample for humidity at level 1 (lowest RH level).

## 3. Results and Discussion

### 3.1 XRD Analysis

The crystallinity of the sample is clearly evident by the sharper diffraction peaks at respective diffraction angles which can be readily indexed for its rutile tetragonal structure of the as-prepared SnO<sub>2</sub> powder, as given in Figure 1. The obtained rutile phase is comparable with the standard

JCPDS data (card no: 41-1445). The sample exhibited only the tetragonal phase and the peaks appear at 2θ = 26.81, 33.84, 38.12, 51.21, 54.23, 62.32, 66.35. The decrease of broadening indicates the growth of the crystallite size from minimum to maximum value, but average crystallite size is around 46 nm for the as-prepared powder. No peaks arising from other crystallised impurities such as TiO<sub>2</sub>.TiSnO<sub>3</sub> in Mn-doped samples, the peak shifting in the higher angle indicating the Mn ions substitution in the SnO<sub>2</sub> lattice site. Besides, the calculated lattice parameters decrease with the increase of Mn content (Table 1). This is due to similar ionic radius of Mn<sup>2+</sup> ion (0.80 Å) with respect to the Sn<sup>4+</sup> ion radius (0.69 Å) [10].

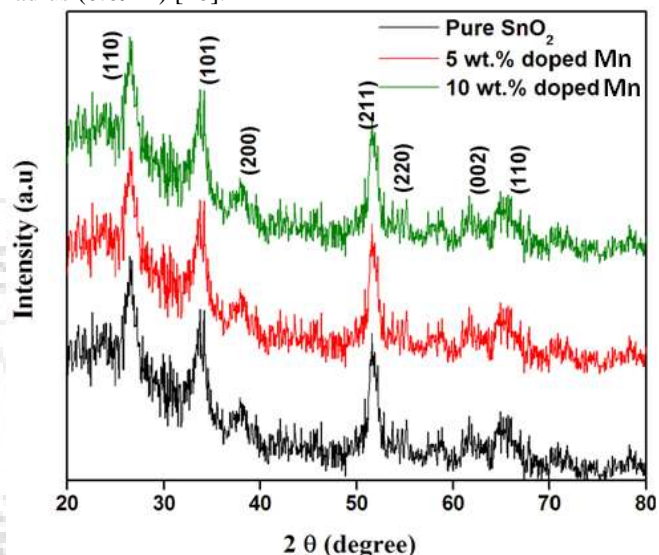
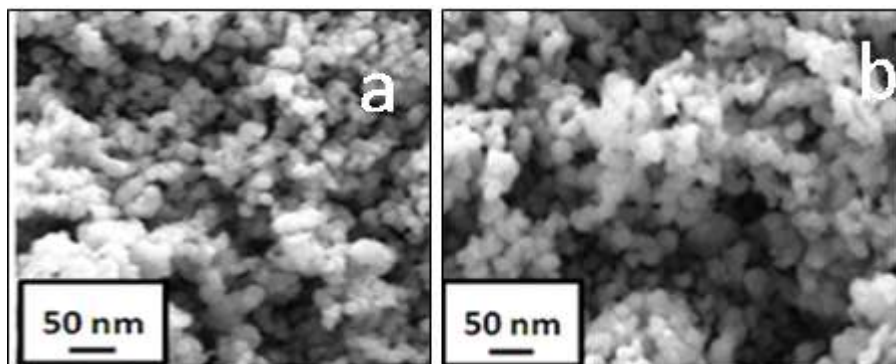


**Figure 1:** Powder XRD pattern of SnO<sub>2</sub> nanoparticles with different Mn content (a) pure SnO<sub>2</sub>(b) Mn 5 wt % and (c) Mn 10 wt %

**Table 1:** Lattice parameters and crystallite size of SnO<sub>2</sub> nanoparticles with different Mn concentrations

Mn Concentrations (Wt %)	Crystallite size (nm)	Lattice Parameters		Cell Volume (Å <sup>3</sup> )
		a(Å)	c(Å)	
0	46	4.7968	3.1901	71.23
5	42	4.7883	3.1934	70.67
10	32	4.7791	3.1893	69.12

### 3.2 Transmission electron Microscopic Analysis



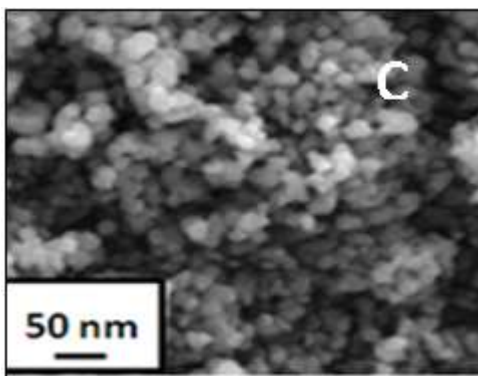


Figure 2: TEM image of a) pure SnO<sub>2</sub> (b) Mn 5 wt % c) Mn 10 wt %

Figure 2 shows TEM micrograph of pure and Mn doped SnO<sub>2</sub> powder, which reflects the highly agglomerated powder having nearly spherical nanocrystals with facets of size around 50 nm. The particle size observed by TEM are in good agreement with that estimated by X-ray diffraction. There is no change in morphology after addition of Mn, still it remains spherical shaped. This study again favors for the evolution of tetragonal phase due to high degree of agglomeration which can reduce the surface energy.

### 3.3 UV-Vis Transmission Spectra Analysis

UV-visible spectral study is performed to determine the optical property of the pure and doped samples. Figure 3 a) shows the UV-Vis transmission spectra analysis of pure and Mn-doped SnO<sub>2</sub> nanoparticles. In pure samples, the absorption edge was estimated to be 368 nm. Further, it increases and shifted towards the higher wavelength for Mn-doped samples. It indicates that the optical property of pure SnO<sub>2</sub> is significantly enhanced by Mn doping. The red shift in the absorption edge is due to the band gap of pure SnO<sub>2</sub>. The energy gap is calculated as 3.67 eV, 3.42 eV and 3.25 eV for pure and Mn-doped SnO<sub>2</sub> (5wt%,10wt%) samples respectively (Figure 3 b). The decrease in band gap energy confirm the substitution of Mn<sup>+</sup> ion in the SnO<sub>2</sub> host lattice and forms the intermediate energy level between the conduction and valance band of pure SnO<sub>2</sub>.

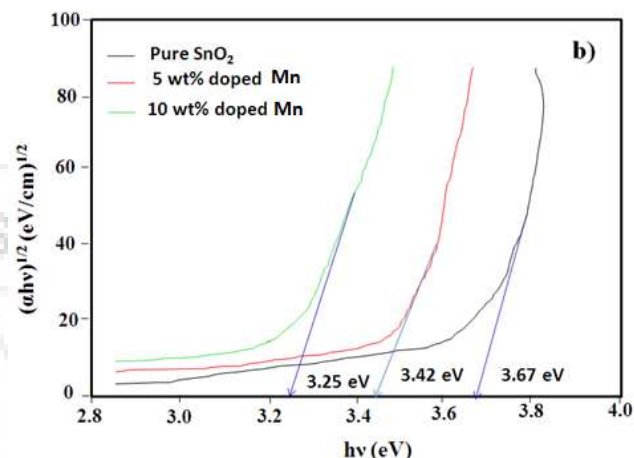
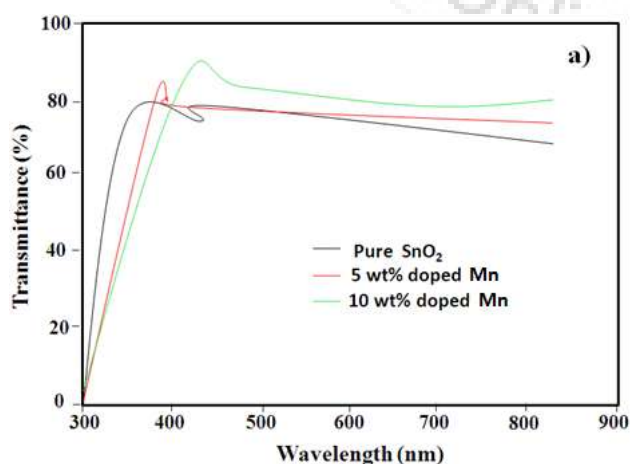


Figure 3: UV-Vis spectra of SnO<sub>2</sub> nanoparticles with different Mn content (a) transmittance spectra (b) band gap energy determination

### 3.4 FTIR Spectra Analysis

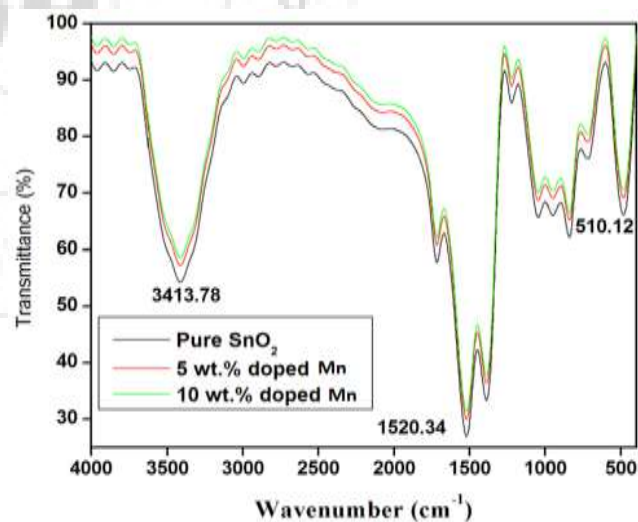


Figure 4: FTIR spectra of pure and Mn-doped SnO<sub>2</sub> nanoparticles

The FTIR spectra for pure as well as Mn doped SnO<sub>2</sub> particles were recorded using the KBr pellet technique in the range 500–4000 cm<sup>-1</sup>. Figure 4 shows FTIR spectra of pure and Mn-doped SnO<sub>2</sub> (5 wt % and 10 wt %) samples at room temperature. The absorption bands observed at 3413.78 cm<sup>-1</sup> is owing to stretching vibration of surface hydroxyl. The vibrations at 1609.21cm<sup>-1</sup> correspond to the tin-hydroxyl (Sn–OH) bond [12]. The sharp band appeared between 400



$\text{cm}^{-1}$  and  $700 \text{ cm}^{-1}$  is associated to the O–Sn–O bridge functional groups of  $\text{SnO}_2$ , which confirms the presence of  $\text{SnO}_2$  in the crystalline phase [13]. No other extra peaks were detected in the Mn-doped samples, this suggest that Mn has substitutionary doped with regular lattice site of  $\text{SnO}_2$ .

### 3.5 Humidity sensor test

The resistance values as a function of humidity from 10% RH to 90% RH at room temperature is shown in Figure 5. The resistance value is found to decrease with increase of relative humidity. It indicates that electrons are trapped by surface defects namely oxygen vacancies and released when water molecules are adsorbed onto the defect sites [14]. The sensitivity of both pure and Mn doped  $\text{SnO}_2$  samples as a function of relative humidity is shown in Figure 6. The sensitivity is estimated for various relative humidity (RH 10% to RH 90%). It reveals that sensitivity is linearly increases with increase of relative humidity. The Mn (10 wt%) doped sample demonstrate high sensitivity and stability when compared with pure sample. The response and recovery performance play vital role in determining efficiency of humidity sensors [13]. The response time ( $\tau_{\text{res}}$ ) of the  $\text{SnO}_2$  sensor defined as time taken to decrease up to minimum resistance (90%) when relative humidity exist inside the chamber. On the other hand, the recovery time ( $\tau_{\text{rec}}$ ), is defined as time required to increase resistance up to 90% in the absence of relative humidity [4]. Figure 7 displays the response and recovery graph for both pure and Mn doped  $\text{SnO}_2$  sensor as a function of relative humidity. The average response time is 52 s and recovery time is 40 s for pure  $\text{SnO}_2$ , similarly the average response and recovery time was found to be 45 and 20 s for Mn (10 wt%) doped  $\text{SnO}_2$  sensor. Hence, these interesting research findings promote that Mn– $\text{SnO}_2$  nanoparticles could be a potential candidate for high performance humidity sensing applications. This response is mainly due to the large oxygen vacancies and surface area which resulted in high sensitivity.

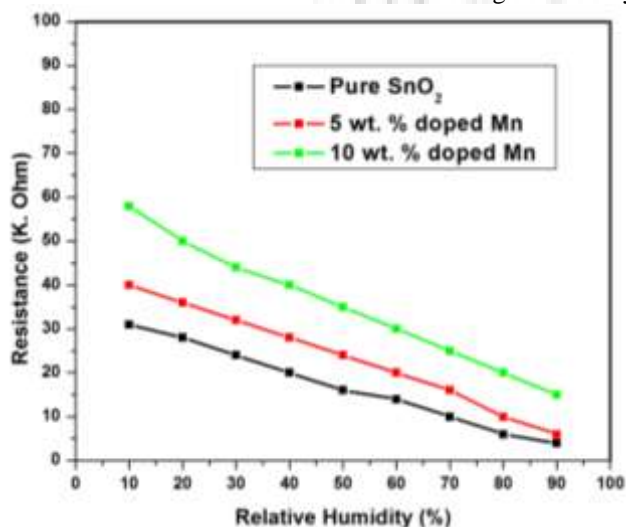


Figure 5: Change in resistance of pure and Mn doped  $\text{SnO}_2$  sensor as a Function of relative humidity

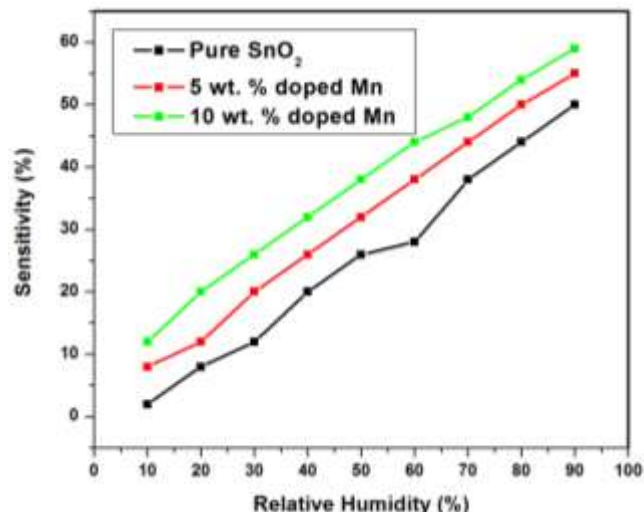


Figure 6: Sensitivity of pure and Mn doped  $\text{SnO}_2$  sensor as a function of Relative humidity

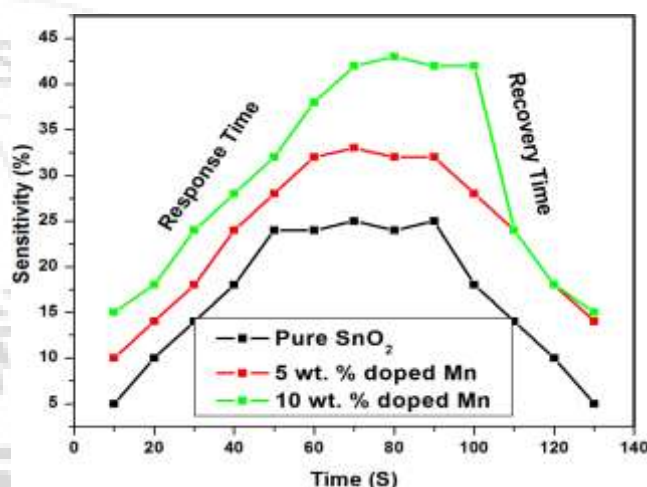


Figure 7: Response and recovery time of pure and Mn doped  $\text{SnO}_2$  sensor as a function of relative humidity

## 4. Conclusion

A one step facile method of nanoparticle synthesis was used to synthesize  $\text{SnO}_2$  and Mn-doped  $\text{SnO}_2$ . The samples were successfully synthesized by hydrothermal method. The XRD results showed the strong evidence of the partial substitution of Mn atom into  $\text{SnO}_2$  structure. The elemental analysis confirmed the presence of Mn atom which was inserted into Sn atom. FTIR experiment confirmed the Sn-O and Sn-Mn-O stretching vibration. TEM experiment exhibited the uniform shape and size of  $\text{SnO}_2$  and Mn-doped  $\text{SnO}_2$ . The energy gap were analyzed from UV – VIS which enhance the band gap with Mn doping due to the quantum confinement effects. The response time of Mn (10 wt%) doped  $\text{SnO}_2$  sensor is significantly high than the pure  $\text{SnO}_2$ . These interesting findings of this research paper reveal that Mn– $\text{SnO}_2$  nanoparticles is a suitable material for elevated performance for as humidity sensor.

## References

- [1] B Liu, C W Cheng, R Chen, Z X Shen, HJ Fan, HDSun (2010) Fine structure of ultraviolet

- photoluminescence of Tin Oxide nanowires. *J. Phys. Chem. C* 114:3407–3410.
- [2] S Mehraj, M S Ansari, Alimuddin (2015) Structural, electrical and magnetic properties of (Fe, Co) codoped SnO<sub>2</sub> diluted magnetic semiconductor nanostructures. *Physica E* 65:84–92.
- [3] J S Lee, S K Sim, B Min, K Cho, S W Kim, S Kim (2004) Structural and optoelectronic properties of SnO<sub>2</sub> nanowires synthesized from ball-milled SnO<sub>2</sub> powders. *J. Cryst. Growth* 267:145–149.
- [4] G Faglia, C Baratto, G Sberveglieri, M Zha, AZappettini (2005) Adsorption effects of NO<sub>2</sub> at ppm level on visible photoluminescence response of SnO<sub>2</sub> nanobelts. *Appl. Phys. Lett.* 86:011923.
- [5] G Xu, Y W Zhang, X Sun, C L Xu, C H Yan (2005) Synthesis, structure, texture, and CO sensing behavior of nanocrystalline Tin Oxide doped with Scandia. *J. Phys. Chem. B* 109:3269–3278.
- [6] Y Wang, J Y Lee (2004) Molten salt synthesis of Tin Oxide nanorods: morphological and electrochemical features. *J. Phys. Chem. B* 108:17832–17837.
- [7] H Sugimoto, H Tsukube, K Tanaka (2004) Immobilization of a high-valent Rhenium complex on an Indium-doped Tin-Oxide electrode: enhanced catalytic activity of a trans-Dioxorhenium(V) complex in electrochemical oxidation of alcohols. *Eur. J. Inorg. Chem.* 23:4550–4553.
- [8] N Q Jia, Q Zhou, L Liu, M M Yan, Z Y Jiang (2005) Direct electrochemistry and electrocatalysis of horseradish peroxidase immobilized in sol-gel derived tin oxide/gelatin composite films. *J. Electroanal. Chem.* 580:213–221.
- [9] S Mehraj, M S Ansari, Alimuddin (2015) Rutile type SnO<sub>2</sub> thin films annealed at different temperature: structural, dielectric, impedance and ferromagnetic properties. *Thin Solid Films* 589:57–65.
- [10] F Gu, S F Wang, C F Song, M K Lu, Y X Qi, G J Zhou, D Xu, D R Yuan (2003) Synthesis and luminescence properties of SnO<sub>2</sub> nanoparticles. *Chem. Phys. Lett.* 372:451–454.
- [11] S Mehraj, M S Ansari, Alimuddin (2013) Structural, dielectric and complex impedance properties of Cd doped SnO<sub>2</sub> nanoparticles. *J. Nanoeng. Nanomanuf.* 3:1–8.
- [12] Z M Tian, S L Yuan, J H He, P Li, S Q Zhang, C H Wang, Y Q Wang, S Y Yin, L Liu (2008) Structure and magnetic properties in Mn doped SnO<sub>2</sub> nanoparticles synthesized by chemical co-precipitation method. *J. Alloys Compd.* 466:26–30.
- [13] B Sathyaseelan, K Senthilnathan, T Alagesan, R Jayavel, K Sivakumar (2010) A study on structural and optical properties of Mn and Co-doped SnO<sub>2</sub> nanocrystallites. *Mater. Chem. Phys.* 124:1046–1050.
- [14] M. Anbia, F. Khosravi, Synthesis of nanoporous TiO<sub>2</sub> materials using a doubly surfactant system and applying them as useful adsorbent, *Radiat. Eff. Defects Solids* 164 (2009) 541–550.
- [15] S. Agarwal, G.L. Sharma, Humidity sensing properties of (Ba, Sr)TiO<sub>3</sub> thin films grown by hydrothermal–electrochemical method, *Sens. Actuators B* 85 (2002) 205–211.
- [16] Wang X-H, Ding Y-F, Zhang J, Zhu Z-Q, you S-Z, Chen S-Q, Zhu J (2006) *Sens Actuators B* 115:421–427
- [17] Ates T, Tatar C, Yakuphanoglu F (2013) *Sens Actuators* 190:153
- [18] M.-M. Bagheri-Mohagheghia, b, N. Shahtahmasebia, M.R. Alinejada, A. Youssefic, M. Shokooh-Saremid "The effect of the post-annealing temperature on the nano-structure and energy band gap of SnO<sub>2</sub> semiconducting oxide nano-particles synthesized by polymerizing–complexing sol–gel method", *Physica B*, Vol.403, pp. 2431–2437, 2008.
- [19] Du, F., Guo, Z., Li, G. "Hydrothermal synthesis of SnO<sub>2</sub> hollow microspheres" *Mater. Lett.* Vol.59, pp. 2563, 2005.
- [20] Raman Mishra and P. K. Bajpai "Synthesis, Dielectric and Electrical Characterization of SnO<sub>2</sub> Nano-particle Prepared by Co-precipitation Method" *Journal of International Academy of Physical Sciences* Vol. 14 No.2, pp. 245–250, 2010.
- [21] "Microwave synthesis, characterization and humidity sensing properties of single crystalline Zn<sub>2</sub>SnO<sub>4</sub> nanorods Mathivanan Parthibavarman, Kaliyan Vallalperuman, Chinnathambi Sekar, Gopal Rajarajan, Thanagaraju Logeswaran. Volume 95, September 2013, Pages 76
- [22] Mathivanan Parthibavarman, Kaliyan Vallalperuman, Chinnathambi Sekar, Gopal Rajarajan, Thanagaraju Logeswaran. *Nano Vision*, Vol.3 (2), 44–52 (2013) *Nano Vision*, Vol.3, Issue 2, 30 June, 2013, Pages (44–92) Microwave Assisted Technique for Synthesizing ZnCdO. High-sensitivity humidity sensor based on SnO<sub>2</sub> nanoparticles .
- [23] Vivek Kumar, Shashwati Sen, K.P. Muthe, N. K. Gaur, S. K. Gupta, J. V. Yakhmi, *Sens. Actuators B: Chemical* 138, 587 (2009).